coatings

MDPI

Article

Feasibility Analysis of Resource Application of Dry Flue Gas Desulfurization Ash in Asphalt Pavement Materials

Kai Li, Zhigang Zhou *, Yinghui Zhang * and Ronghua Ying

School of Traffic and Transportation Engineering, Changsha University of Science and Technology, No. 2-960, Wanjiali Rd (South), Yuhua District, Changsha 410114, China; likai_cs@163.com (K.L.); 14773900488@163.com (R.Y.)

* Correspondence: zhou_zgcs@163.com (Z.Z.); 20001030021@stu.csust.edu.cn (Y.Z.)

Abstract: To verify the feasibility of applying dry flue gas desulfurization ash (DFGDA) to asphalt pavement materials, the asphalt mastic (filler and asphalt composition) prepared by adding different proportions of DFGDA and LSP (limestone powder) into 70# matrix asphalt was studied experimentally. The asphalt mastics were subjected to the penetration test, the softening point test, and the ductility test. Moreover, the rheological properties of asphalt mastic were evaluated with dynamic shear rheometer (DSR) tests and bending beam rheometer (BBR) tests. An interaction ability index C-value based on the Palierne model was proposed to evaluate the interaction ability between DFGDA and asphalt. The influence of DFGDA asphalt on the interaction ability of matrix asphalt was observed and evaluated using Fourier transform infrared spectroscopy (FTIR) and scanning electron microscopy (SEM). The results showed that with the increasing proportion of DFGDA, the penetration of asphalt mastic gradually decreased, the softening point increased, and the ductility slightly decreased. At the same temperature, the dynamic shear modulus G* of the asphalt mortar significantly increased with increasing DFGDA content. The incorporation of DFGDA negatively affected the low-temperature plastic deformation resistance of asphalt, but the impact was weakened with the growing DFGDA amount and the powder mastic ratio. The combination mode of DFGDA and matrix asphalt depends on the physical blending, and their interaction ability mainly depends on the miscibility between DFGDA and matrix asphalt. In conclusion, DFGDA can be utilized as a novel filler in asphalt pavement materials.

Keywords: asphalt mastic; dry flue gas desulfurization ash; limestone; rheological properties; interaction ability; performance evaluation

Citation: Li, K.; Zhou, Z.; Zhang, Y.; Ying, R. Feasibility Analysis of Resource Application of Dry Flue Gas Desulfurization Ash in Asphalt Pavement Materials. *Coatings* **2024**, *14*, 591. https://doi.org/10.3390/coatings14050591

Academic Editor: Andrea Nobili

Received: 3 April 2024
Revised: 30 April 2024
Accepted: 7 May 2024
Published: 9 May 2024

1. Introduction

Steelmaking and power generation worldwide are still mainly powered by burning fossil resources. However, the burning of fossil resources results in large amounts of sulfur dioxide and other environmentally harmful gases and contributes to climate warming and acid rain, which is harmful to the growth of plants and animals and even human lives [1,2]. To reduce sulfur dioxide emissions, desulfurization and dust removal measures have been adopted in the steel and power industries. The commonly used desulfurization technologies can be classified into dry desulfurization, semi-dry desulfurization, and wet desulfurization, with each including various processes [3,4]. Among the dry desulfurization technologies, the circulating fluidized bed flue gas desulfurization (CFB-FGD) is called "ultra-clean" desulfurization. Owing to its high desulfurization efficiency, low energy consumption, small investment and space requirement, integration of desulfurization and dust removal, and significant reduction in solid particulate emissions, it has been widely used in steel and other industries in recent years [5]. However, the dry flue gas desulfurization ash (DFGDA), a byproduct of this process, is challenging to recycle and is mainly deposited in piles and landfills, with only a small portion effectively used [6]. The

difficulty in recycling DFGDA results in the waste of potential resources and environmental pollution because DFGDA contains abundant calcium sulfate hemihydrate, The unstable calcium sulfite during utilization is easily and slowly oxidized to calcium sulfate in humid environments and then decomposed to sulfur dioxide under acidic or high-temperature conditions [7,8]. Therefore, the application of DFGDA in asphalt pavement materials has rarely been reported [9,10].

In the United States, DFGDA is mainly used for soil improvement and stabilization, mining, and waste solidification because of its gelling properties [11]. Burgess-Conforti et al. [12] used DFGDA as a soil amendment in a one-year field trial. The results showed that DFGDA increased the content of trace elements (e.g., Ca, S, and Na) in the soil, with its concentration decreased to preapplication levels within 3 to 6 months. Chen et al. [13] employed DFGDA to remediate abandoned acidic coal mines and to monitor surface runoff and plant and soil microbial properties in the long term. The results indicated that the pH values of surface runoff were maintained at above 7. The trace element concentrations of Ca, S, and B in soil and plant tissues exhibited a trend of first increasing and then decreasing, while heavy metal concentrations showed no significant increase. Moreover, the bacterial populations, diversity, and microbial biomass were significantly enhanced in the DFGD-remediated restored coal mine area compared with the adjacent untreated area. Therefore, using DFGDA can restore the mine ecology without environmental impairment [14]. Unlike the United States, DFGDA solid waste in China is mainly used in the construction industry. Zhang et al. [15] autoclaved bricks by mixing 77% dry desulfurization ash, 20% CFBC slag, and 3% cement and found no formation of gypsum dihydrate and calcium alumina in the autoclaved bricks, avoiding destructive expansion and presenting good long-term volume stability with compressive strength up to 14.3 MPa. Feng et al. [16] chose desulfurization ash as the main raw material to prepare a novel green grouting fire prevention material. The results demonstrated excellent flame retardancy and performance of the prepared material. Wu et al. [11] fabricated autoclaved aerated concrete using dry desulfurization ash as a cement retarder. It was found that the ash could reduce water consumption and increase the pile density by changing the macroscopic pore structure of concrete, thus improving the concrete strength. Li et al. [17] ground and modified circulating fluidized bed combustion (CFBC) and found that CFBC desulfurization ash was a self-consolidating material. Its 28 day compressive strength was comparable to that of pure cement mortar, and the modified CFBC desulfurization ashes were suitable as cement admixture due to their high activity. According to the Chinese National Standard, the admixture of desulfurization ash in the blended cement was controlled within 30% to reach a strength grade of 32.5 or 42.5. Sheng et al. [18] also concluded that the addition of CFBC fly ash prolonged the initial setting time due to its self-gelling properties. Duan et al. [19] showed that the ternary hydrated gel system containing fly ash, flue gas desulfurization (FGD) gypsum, and steel slag had better performance with the highest 28 day compressive strength.

Applying industrial waste as filler in asphalt mixture can address the problem of industrial waste disposal and solid waste resource reuse [20]. DFGDA has not been reported in the application of asphalt and asphalt mixtures, but FGD byproducts similar to DFGDA have been identified in some studies. For example, Cloutier et al. [21] added spray dryer absorbers (SDA) to asphalt mixtures at a filler replacement rate of 10% and tested the aging, fatigue, and low-temperature crack resistance of asphalt mixtures. SDA and DFGDA are FGD byproducts produced by different desulfurization processes. The results showed that SDA did not compromise the compatibility of asphalt mixtures. Instead, it improved their aging resistance, water stability performance, and fatigue life. Bautista et al. [22] concluded that coal combustion byproducts, including fly ash, bottom ash, boiling slag, and FGD materials, increased the high-temperature deformation resistance of asphalt materials. The aging resistance and fatigue properties were also improved with the addition of SDA. Mistry and Kumar Roy [23] reported that the joint substitution of 4% rice husk ash and 6% Class F fly ash for mineral dust as a filler improved the deformation resistance and water damage resistance of asphalt mixtures. However, the further increase in the substitution

ratio led to a deterioration in the performance of asphalt mixtures. Chen et al. [24] replaced LSP with calcium sulfate-based desulfurization ash as a filler for asphalt mixtures for related experiments. The results indicated that this ash enhanced the high-temperature road performance, but slightly reduced the water stability performance of asphalt mixtures.

Asphalt mastic is a binary system composed of filler and matrix asphalt, playing a crucial role in the asphalt mixture. Its composition and ratio directly affect the macro road performance of asphalt mixtures [25]. Therefore, studying asphalt mastic is critical to improving the performance of asphalt mixtures. In this paper, the physicochemical properties of DFGDA in the circulating fluidized bed were first investigated. Afterward, the rheological properties of the asphalt mastic with varying amounts of DFGDA and the corresponding action mechanism were studied using desulfurization ash as a new type of filler in asphalt mastic. The findings of this study can provide a theoretical and experimental basis for the application of desulfurization ash in asphalt mastic.

2. Materials and Methods

2.1. Raw Materials

2.1.1. Asphalt

In the test, Shell 70# road petroleum asphalt was selected. The basic performance indicators were measured according to the "Testing Procedures for the Mixing of Asphalt and Asphalt Mixtures for Highway Engineering". The test results are shown in Table 1.

Table 1. Basic performance of 70# matrix asphalt used in the test.

Test Items	Unit	Test Results	Technical Requirements	Single Conclusion
Density (15 °C)	--	1.013	--	/
Penetration (25 °C, 100 g, 5 s)	0.1 mm	72	60–80	Qualified
Softening point	°C	47.5	≥46	Qualified
Ductility (15 °C)	cm	>100	≥100	Qualified
Kinematic Viscosity (60 °C)	Pa.s	190	≥180	Qualified
Wax	%	<2.2	≤2.2	Qualified

2.1.2. Fillers

DFGDA and LSP were used as fillers in the test. DFGDA was supplied by a steel mill, and the basic properties of the fillers are shown in Table 2.

Table 2. Physical and technical indicators of LSP and DFGDA.

Sample Name	Particle Size (μm)			Apparent Density (g/cm^3)	Specific Surface Area (m^2/g)	Hydrophilic Coefficient
	D(10)	D(50)	D(90)			
LSP	1.397	14.086	75.005	2.70	1.37	0.55
DFGDA	1.390	6.231	17.323	2.54	2.79	0.81

Table 2 shows that DFGDA has a slightly smaller particle size and a larger specific surface area than LSP. The apparent density of DFGDA is 94% that of LSP. Lower density indicates more DFGDA particles per unit mass, larger volume, greater total surface area, and more contact of asphalt with the particles, which helps to improve the particle asphalt bond, resulting in a better performance of the mixture. The hydrophilicity coefficient is the ratio between the volume in water and the volume in kerosene, which is used to evaluate the adhesion performance of fillers and asphalt binders. The hydrophilic coefficient of DFGDA was 1.47 times greater than that of LSP, indicating the stronger hydrophilic ability of DFGDA. However, DFGDA and LSP meet the requirement of the Chinese specifications for a hydrophilic coefficient of not more than 1.

2.2. Preparation of Asphalt Mastic

LSP and DFGDA were sieved through a 0.075 mm square hole sieve, and the part below 0.075 mm was selected for subsequent tests. A total of 300 g of base asphalt was weighed. According to the mass ratio of filler to asphalt, which is 0.8, 1, and 1.2, a certain amount of LSP was weighed and mixed with a high speed shear at 150 °C. The asphalt mastic was prepared at a shear rate of 500 r/s for 10 min and then at 3000 r/s for 20 min, during which the effect of asphalt heating and aging was ignored. By replacing the LSP with an equal mass of DFGDA, five groups of asphalt mastics with different powder mastic ratios were prepared and marked as T_0, T_2, T_5, T_8, and T (pure DFGDA), corresponding to DFGDA admixtures of 0% (pure LSP), 20%, 50%, 80%, and 100% (pure DFGDA), respectively.

During the preparation of DFGDA asphalt mastic, it was difficult to mix the asphalt and completely dissolve DFGDA when the mass ratio of fillers to asphalt reached 1.2 and 100% of DFGDA was added to the asphalt LSP. As a result, the mastic could not be prepared and shaped because the desulfurization ash completely absorbed the light components of the asphalt, causing it to harden and lose its fluidity.

2.3. Preparation of Asphalt Mastic

2.3.1. Basic Performance

To quantitatively evaluate the influence law of DFGDA on the macroscopic physical properties of asphalt, asphalt mastic with different amounts of DFGDA was tested regarding penetration, ductility, and softening point.

2.3.2. Dynamic Shear Rheology

The complex shear modulus G*, phase angle δ, and rutting resistance factor G*/sinδ of asphalt mastic with different DFGDA admixtures were determined using a dynamic shear rheometer (DSR). The high-temperature performance of the asphalt mastic was evaluated. The test was conducted in strain controlled mode with strain set at 12% and frequency at 10 rad/s. A test plate with a diameter of 25 mm was selected, with a 1 mm spacing between two parallel plates. The test temperature was set at 58 °C and increased by 6 °C until the specimen failed [26].

2.3.3. Multiple Stress Creep Recovery (MSCR)

After short-term aging, a DSR was used to perform repetitive MSCR on asphalt mastic specimens. The test temperature was set at 70 °C, with a loading cycle of 1 s of creeping loading and 9 s of unloading recovery. The stress of 0.1 kPa was first applied and repeated 10 times, and then the stress of 3.2 kPa was used for 10 cycles. The strain recovery ratio R and the irrecoverable creep flexibility Jnr were calculated according to the strain value changes at the end of the cycle. The permanent deformation resistance of asphalt mastic was evaluated in this way [27].

2.3.4. Bending Beam Rheometer (BBR) Tests

To explore the anti-cracking performance of asphalt mastic with different filler additions at low temperatures, the creep response at −6, −12, and −18 °C was evaluated using the BBR test. (ASTM D 6648). The bending creep modulus S and creep rate m were tested to evaluate the low-temperature crack resistance of asphalt mastic [28].

2.3.5. Scanning Electron Microscopy (SEM)

A Hitachi S-4800 high-resolution field emission scanning electron microscope was used to perform SEM tests on three asphalt slurries (i.e., T_0, T_5, and T) to observe the microscopic distribution morphology of LSP and DFGDA in asphalt [29].

2.3.6. Fourier Transform Infrared Spectroscopy (FTIR)

The infrared spectra of the filler, matrix asphalt, and asphalt mastic with different amounts of DFGDA were tested using a Bruker TENSON II infrared spectrometer at

wavelengths from 650 cm^{-1} to 4000 cm^{-1} with a resolution of 4 cm^{-1}. In addition, the functional group variations of different specimens and the possible chemical reactions were explored by analyzing the changes in the absorption peaks of the main functional groups [30].

2.3.7. Evaluation Indicators for Asphalt-Filler Interaction Based on Palierne Modeling

For the prediction of rheological properties of multiphase blended materials, researchers have developed various prediction models, among which the Palierne model is the most widely used [31], as shown in Equation (1).

$$G_c^*(\omega) = G_m^*(\omega)\frac{1+3\sum_i \phi_i H_i(\omega)}{1-2\sum_i \phi_i H_i(\omega)} \quad (1)$$

where $G_c^*(\omega)$ is the complex shear modulus of the multiphase blend (Pa); $G_m^*(\omega)$ is the complex shear modulus of the continuous phase (Pa); ϕ_i is the volume fraction of the dispersed phase particles with a radius of Ri (%); and is normalized to unity for rigid dispersed phase particles $H_i(\omega)$, this can be calculated using Equation (2).

$$H_i(\omega) = \frac{4(\alpha/R_i)[2G_m^*(\omega)+5G_i^*(\omega)]+[G_i^*(\omega)-G_m^*(\omega)][16G_m^*(\omega)+19G_i^*(\omega)]}{40(\alpha/R_i)[G_m^*(\omega)+G_i^*(\omega)]+[2G_i^*(\omega)+3G_m^*(\omega)][16G_m^*(\omega)+19G_i^*(\omega)]} \quad (2)$$

where α is interfacial tension (N/m), $G_i^*(\omega)$ is the complex shear modulus of the dispersed phase (Pa).

Graebling and Muller [32] suggested that the particle size distribution of the dispersed phase could be replaced by an average diameter representing the filler volume. Thus, the Palierne model can be rewritten as Equation (3).

$$G_c^*(\omega) = G_m^*(\omega)\frac{1+3\sum_i \phi H_i(\omega)}{1-2\sum_i \phi H_i(\omega)} \quad (3)$$

When the dispersed phase is hard solid particles, it can be approximated that the $G_i^*(\omega) \to \infty$ and $H_i(\omega) = 0.5$, and the Palierne model can be further simplified as Equation (4).

$$G_c^*(\omega) = G_m^*(\omega)\frac{1+1.5\phi}{1-\phi} \quad (4)$$

Asphalt mastic consists of asphalt and filler, which is essentially a multiphase comingled material, and its complex shear modulus can be analyzed using the Palierne model for prediction. According to Ziegel and Romanov [33], when dissipated energy is considered, ϕ in the above equation can be replaced by $\phi_F C$, and Equation (4) can be expressed as Equation (5):

$$G_c^*(\omega) = G_m^*(\omega)\frac{1+1.5\phi_F C}{1-\phi_F C} \quad (5)$$

where ϕ_F is the volume fraction calculated from the mass and density of the packing material, C represents the degree of interaction between the asphalt and filler, and its value is influenced by the chemical composition of the asphalt, the specific surface area of the filler, the particle size, and the mineralogical composition.

The asphalt–filler interaction parameter C-value can be derived via Equation (6):

$$C = \frac{G_c^*(\omega)/G_m^*(\omega)-1}{[1.5+G_c^*(\omega)/G_m^*(\omega)]\phi_F} \quad (6)$$

The conversion relationship between the mass ratio of fillers to asphalt m_1/m_2 and the volume fraction of mineral powder φ_F is given in Equation (7).

$$\phi_F = \frac{(m_1/m_2)/\rho_F}{(m_1/m_2)/\rho_F + \rho_A} \quad (7)$$

where ρ_F, ρ_A is the density of mineral powder and asphalt, respectively, g/cm^3.

3. Results

3.1. Basic Performance Test Results

The conventional performance indexes of asphalt mastic with different amounts of DFGDA are shown in Figures 1–3.

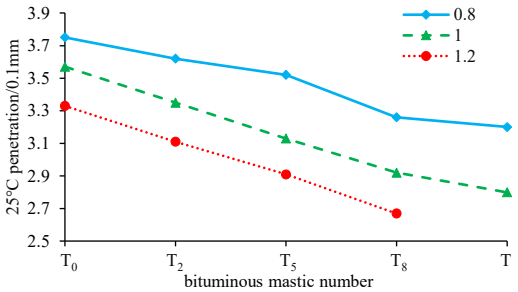

Figure 1. Penetration (25 °C).

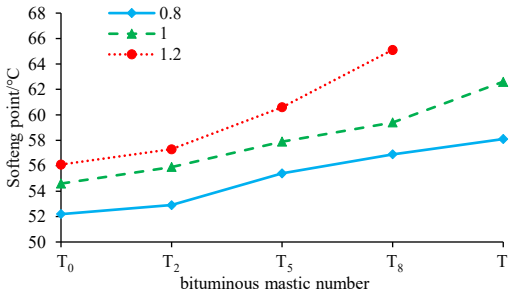

Figure 2. Softening point.

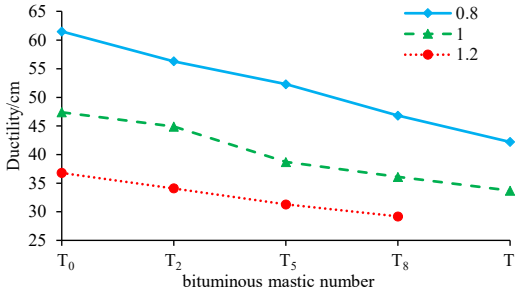

Figure 3. Ductility (10 °C).

Figures 1–3 illustrate that with the increasing mass ratio of fillers to asphalt, the penetration degree of various fillers into the asphalt mastic decreases, the softening point increases, and the ductility decreases. At a mass ratio of 0.8, the permeability of T_0 asphalt increases by 4.8% and 11.2% compared with that at a mass ratio of 1 and 1.2, respectively; the softening point decreases by 4.6 and 7.5%, while ductility decreases by 22.9% and 40.2%. At a constant filler-to-asphalt ratio, a higher content of DFGDA leads to a lower permeability and ductility and a higher softening point. For instance, when the mass ratio of filler to asphalt is 1, increasing the DFGDA content from 0% to 100% can result in a 21.6% reduction in permeability, a 14.7% increase in the softening point, and up to a 28.9% decrease in ductility. These results indicate that the incorporation of fillers enhances the hardness, consistency, and high-temperature deformation resistance of asphalt, with

DFGDA showing significantly higher improvement than LSP. Nevertheless, filler addition does not enhance the low-temperature ductility of asphalt, and the impact of DFGDA on diminishing this property is more pronounced than that of LSP.

3.2. DSR Text Results

3.2.1. High-Temperature Dynamic Rheological Properties

The rheology properties of asphalt mastic play a decisive role in the performance of the asphalt mixture [34]. The SHRP program in the United States indicated that asphalt rheological properties could be expressed in terms of a dynamic shear modulus and phase angle of asphalt at constant temperature or loading time and frequency. Figures 4–6 show the dynamic shear modulus, phase angle, and rutting factor of the asphalt mastic with different amounts of DFGDA at different temperatures.

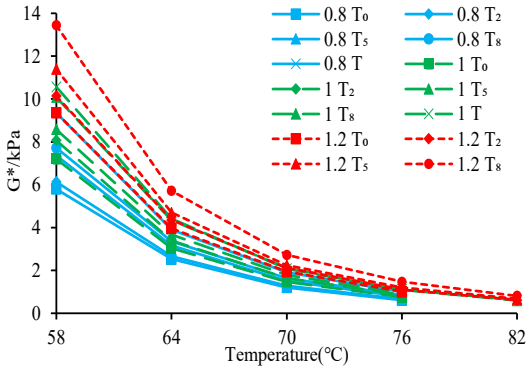

Figure 4. Dynamic shear modulus.

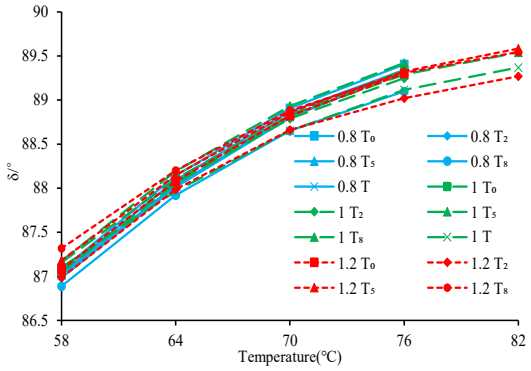

Figure 5. Phase angle.

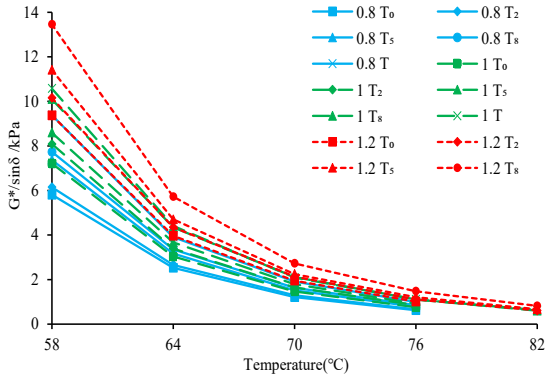

Figure 6. Rutting factor.

As shown in Figure 4, under the same amount of DFGDA, the dynamic shear modulus of the asphalt mastic shows a rapid decline at 58–70 °C, a gradual decrease at 70–76 °C, and enters into a flat stage at 76–82 °C. The results indicate that the asphalt mastic deformation resistance weakened with the elevated temperature. The phenomenon is due to the increase in temperature accelerates the speed of molecular movement, weakening intermolecular van der Waals forces, increasing spacing, transforming asphalt macroscopic performance (from the low-temperature highly elastic state to high-temperature viscous flow state), and decreasing dynamic shear modulus of asphalt mastic. At the same temperature and powder mastic ratio, the dynamic shear modulus of LSP asphalt mastic was the smallest; with the increase in DFGDA admixture, the dynamic shear modulus of asphalt mastic increased, reaching the maximum when the DFGDA admixture was 100%. Consequently, the elastic component became more extensive, and the deformation resistance was improved. These results suggest that the DFGDA addition could improve the high-temperature properties of the asphalt mastic. The phase angles of the asphalt mastic specimens ranged from 86° to 90° within the test temperature, indicating the dominant viscous component and the relatively small elastic component of the asphalt (Figure 5). The rutting factor of the asphalt mastic decreased continuously as the test temperature increased from 58 °C to 82 °C, implying that the rutting factor was influenced by temperature (Figure 6). At the same temperature and powder mastic ratio, the rutting factor of asphalt mastic was greater with higher DFGDA dosing, demonstrating the improved high-temperature deformation resistance of asphalt mastic. Compared with LSP, DFGDA possesses relatively similar surface properties but a larger specific surface area, which enhances adsorption between asphalts and the intermolecular force. Finally, the macroscopic performance of the load under the high-temperature deformation resistance of asphalt mastic was improved.

3.2.2. High-Temperature Dynamic Rheological Properties

Superpave specification of the asphalt bond requires a rutting resistance factor of the original sample asphalt higher than 1 kPa, and the temperature corresponding to this condition is taken as the high-temperature failure temperature to determine the high-temperature PG classification grade of asphalt. By regarding the asphalt mastic as the original asphalt, the temperature corresponding to each asphalt mastic with a rutting resistance factor of 1 kPa was calculated using interpolation using the DSR test results of the previous asphalt mastic, which was the high-temperature failure temperature of the asphalt mastic (Figure 7).

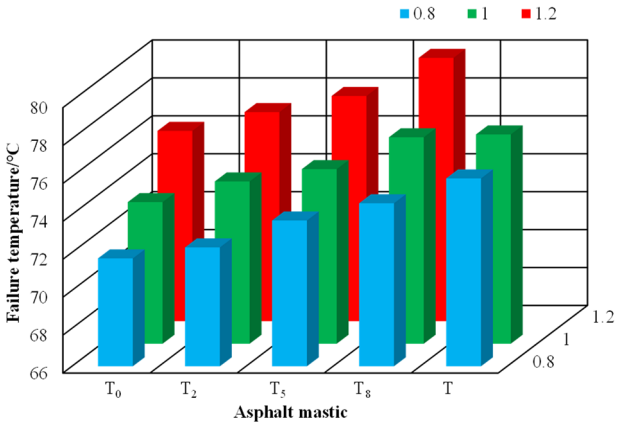

Figure 7. Failure temperature of asphalt mortar with different powder mastic ratio.

As shown in Figure 7, the failure temperature of asphalt mastic is lower than 76 °C when the mass ratio of filler to asphalt is 0.8, but is higher than 76 °C when the mass ratio of filler to asphalt is 1.2. It indicates that a higher mass ratio of fillers to asphalt can lead to a greater high-temperature failure temperature of asphalt mastic under the same conditions. Therefore, the addition of filler can improve the high-temperature performance of asphalt.

The failure temperature of asphalt mastic increases with increasing DFGDA. For example, when the mass ratio of fillers to asphalt was 1, the failure temperature of T_0 was 73 °C, while that of T was 77 °C, with a total increase of 4 °C. This result suggests that DFGDA significantly improved the high-temperature rheological performance of asphalt mastic compared to pure LSP.

3.3. MSCR Test Results

An MSCR test can accurately assess the viscoelastic deformation of asphalt mastic under the action of repeated stress levels. The asphalt mastic produces creep deformation during stress loading, and the elastic deformation and delayed elastic deformation are recovered during the unloading stage, which is called recoverable creep deformation. In contrast, the viscoelastic deformation is unrecoverable, which is defined as residual deformation. MSCR test can simulate the deformation of asphalt pavement under load more realistically. The results are shown in Figures 8–11.

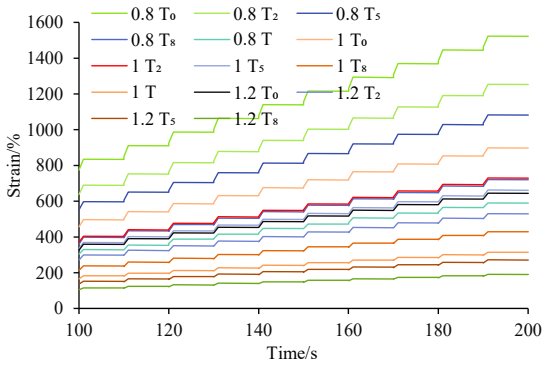

Figure 8. Creep recovery curve (0.1 kPa).

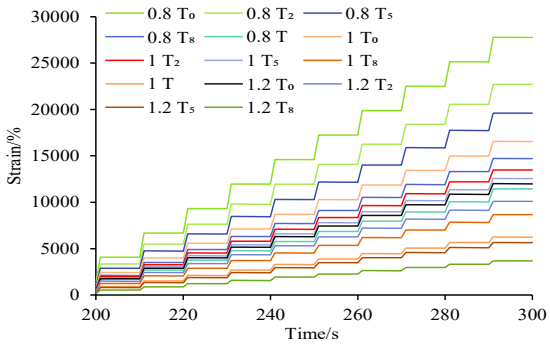

Figure 9. Creep recovery curve (3.2 kPa).

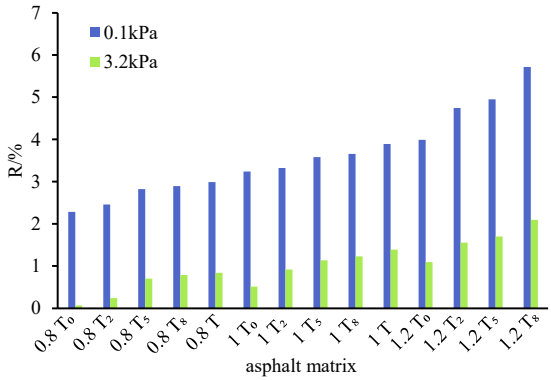

Figure 10. Strain recovery ratio.

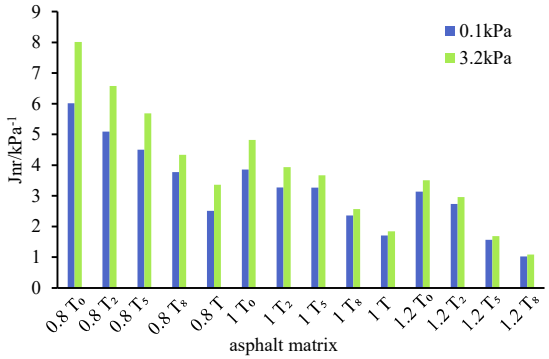

Figure 11. Non-recoverable creep flexibility.

As shown in Figures 8 and 9, the asphalt mastic strain of different DFGDA doses increases with the loading time. Under the same loading time and powder mastic ratio, a higher DFGDA amount leads to a smaller corresponding mastic strain. When the mass ratio of fillers to asphalt was 0.8, the strain generated by T decreased by 61.3% compared with that by T_0 after cycle loading at a stress level of 0.1 kPa. In addition, the cycle loading was reduced by 58.8% after a stress level of 3.2 kPa. These results indicate that DFGDA could significantly improve the asphalt mastic resistance to deformation. As shown in Figure 10, higher loading stress causes a smaller strain recovery ratio of asphalt mastic at a certain number of load actions and powder mastic ratio, implying that a higher load led to a poorer permanent deformation resistance of asphalt mastic. When other conditions were specific, the strain recovery ratio of asphalt mastic gradually increased with increasing DFGDA admixtures, suggesting that the increasing DFGDA admixture increased the strain recovery ratio of asphalt mastic. Compared with LSP asphalt mastic, DFGDA asphalt mastic showed better elasticity and a higher elastic deformation percentage in creep deformation, eventually exhibiting an increasing strain recovery ratio. As shown in Figure 11, at a certain number of load actions and a certain mass ratio of fillers to asphalt, the irrecoverable creep flexibility of asphalt mastic increases with increasing stress, leading to the greater residual deformation of asphalt mastic. These results demonstrate a poor deformation resistance of asphalt mastic. Under other conditions, the irrecoverable creep flexibility of asphalt mastic decreased with the increasing DFGDA admixture, implying that the DFGDA addition could reduce the irrecoverable creep flexibility of asphalt and improve the permanent deformation resistance of the asphalt. This phenomenon could be attributed to the excellent elasticity of DFGDA and greater intermolecular forces within the DFGDA asphalt, which allowed the DFGDA asphalt mastic to form a more substantial damping effect, macroscopically manifesting by the decrease in irrecoverable creep flexibility and increase in strain recovery ratio produced by the asphalt mastic under the same stress.

3.4. BBR Test Results

The low-temperature cracking resistance of asphalt binders was measured based on two indicators (i.e., flexural creep modulus of strength S and creep rate m) through the BBR test. A smaller flexural creep modulus of strength resulted in a more flexible asphalt mastic, greater allowable deformation, and better low-temperature crack resistance. The creep rate characterizes the relaxation performance of asphalt mastic. A larger creep rate indicates a greater internal stress release rate, a stronger relaxation capacity, and better low-temperature crack resistance. The flexural creep modulus of strength and creep rate corresponding to asphalt mastic of different DFGDA admixtures were measured. The results are shown in Figures 12 and 13.

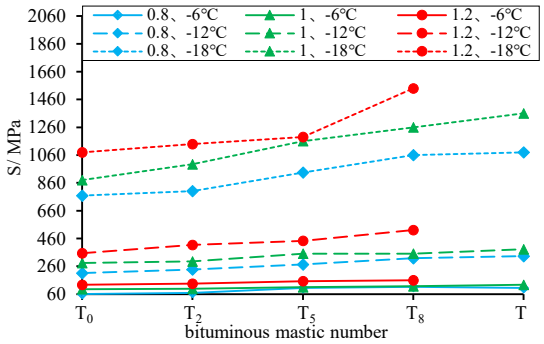

Figure 12. Bending creep stiffness modulus.

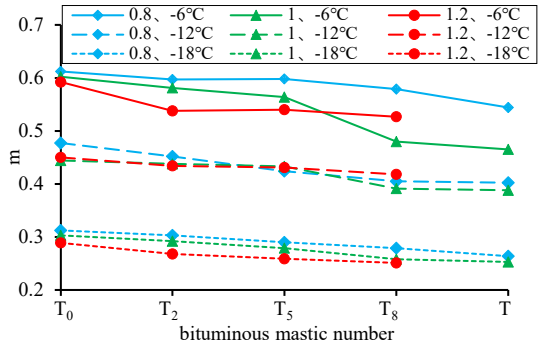

Figure 13. Changes in creep rate over time.

Figures 12 and 13 show that the creep stiffness of the asphalt mortar increases significantly, and the creep rate decreases significantly with increasing temperature, with the most significant decrease in creep rate at 12–18 °C. The results demonstrated that the sensitivity of stiffness modulus and creep rate increased as the temperature decreased, induced by the hardening asphalt. The proportion of viscous components in asphalt was lessened gradually, and the reduction rate rose with decreasing temperature. The content of viscous components in asphalt was positively correlated with the low-temperature performance of asphalt. Under the same temperature and powder mastic ratio, asphalt mastic presented a gradually increased creep modulus and a decreased creep rate with the increasing DFGDA. These results indicate that the incorporation of DFGDA deteriorated the low-temperature performance of asphalt mastic, which is consistent with the ductility test results. At the same temperature, with the mass ratio of fillers to asphalt, the flexural creep modulus of strength significantly increased, while the creep rate showed only a small reduction. When the mass ratio of fillers to asphalt was 1 and 1.2, the creep rate change curve of the DFGDA asphalt mastic presented an intersection. The increase in mass ratio of fillers to asphalt reduced the deformation resistance of asphalt mastic. However, it slightly affected its stress relaxation capacity, revealing the limitations in evaluating the low-temperature performance of DFGDA asphalt mastic using a single value of flexural creep modulus of the strength and creep rate.

4. Evaluation Index Analysis and Microscopic Mechanism of Interaction between Mastic Asphalt and DFGDA

4.1. C-Value

Since a larger C-value indicates that the filler can adsorb asphalt more strongly, the C-value can be used to evaluate the ability of interaction between fillers and asphalt. The interaction indicator C-value calculated with Equation (8) is shown in Figure 14.

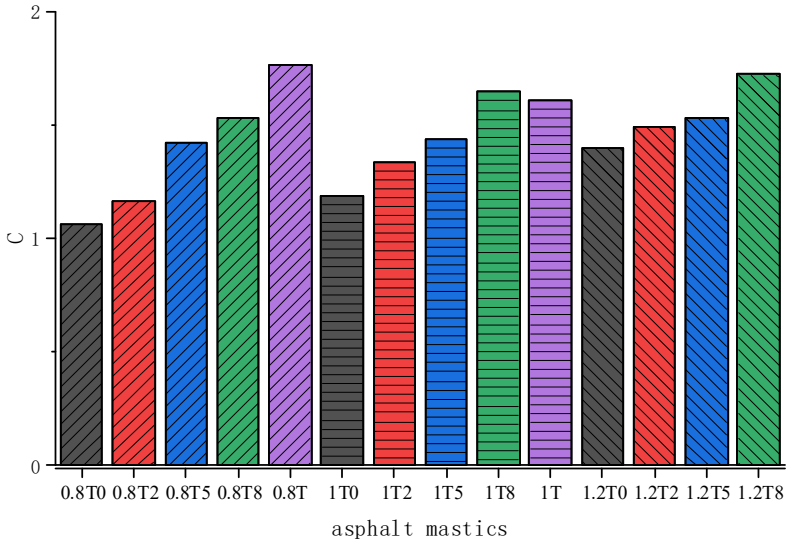

Figure 14. Results of indicator C-value between different fillers and asphalt.

It can be seen from Figure 14 that when the filler composition is consistent, the C value increases with the increase of the powder mastic ratio. Moreover, in the case of T_0, the C-value under a mass ratio of fillers to asphalt of 1 is enhanced by 33% compared to that under a powder mastic ratio of 0.8, while the C-value under a mass ratio of fillers to asphalt of 1.2 is enhanced by 41% compared to that under a powder mastic ratio of 1. It is shown that in the range of 0.8 to 1.2 powder mastic ratio, the elevation of the mass ratio of fillers to asphalt can help improve the ability of interaction between asphalt and filler. Under the same powder mastic ratio, the C-value increased with the increase of DFGDA content in the filler. Compared with mineral powder, the addition of DFGDA can effectively facilitate the interaction between filler and asphalt, which is mainly due to the larger surface area of DFGDA and its increased contact area with asphalt. This contributes to enhancing the physical adsorption between them, leading to superior overall performance.

4.2. SEM Test Results

The microscopic morphology of asphalt mastic T_0 and T was analyzed using SEM, and the results are shown in Figure 15.

As shown in Figure 15, both DFGDA and LSP can be evenly distributed in asphalt. DFGDA and LSP particles were dispersed in asphalt, and their internal voids absorbed the lighter components of asphalt, increasing the asphalt powder binding capacity (i.e., improved interaction ability between asphalt and filler and enhanced high-temperature rheological properties of asphalt). The LSP particles were embedded in the asphalt, and there were certain voids around the DFGDA and asphalt. The existence of voids caused local stress concentration, manifested as a material strength reduction. Therefore, the asphalt mastic ductility and flexural creep modulus of strength decreased to a certain extent with the increase in DFGDA.

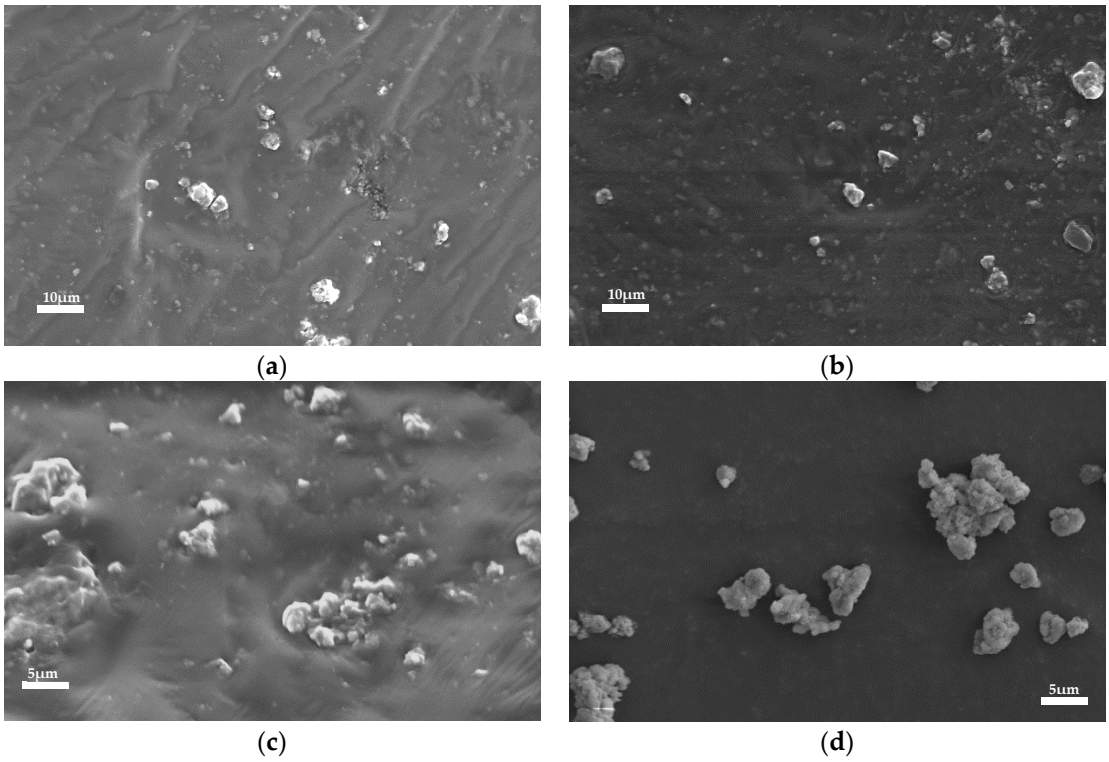

Figure 15. SEM Analysis of Asphalt Mastic Morphology at Different Aging Stages: T_0 and T. (**a**) T_0 asphalt mastic 1000 magnification (10 μm); (**b**) T asphalt mastic 1000 magnification (10 μm); (**c**) T_0 asphalt mastic 2000 magnification (5 μm); and (**d**) T asphalt mastic 2000 magnification (5 μm).

4.3. FTIR Test Results

FTIR was used to test the absorption peak changes of the main functional groups of the filler (LSP and DFGDA), matrix asphalt, and asphalt mastic (T_0, T_5, and T). The results are shown in Figure 16.

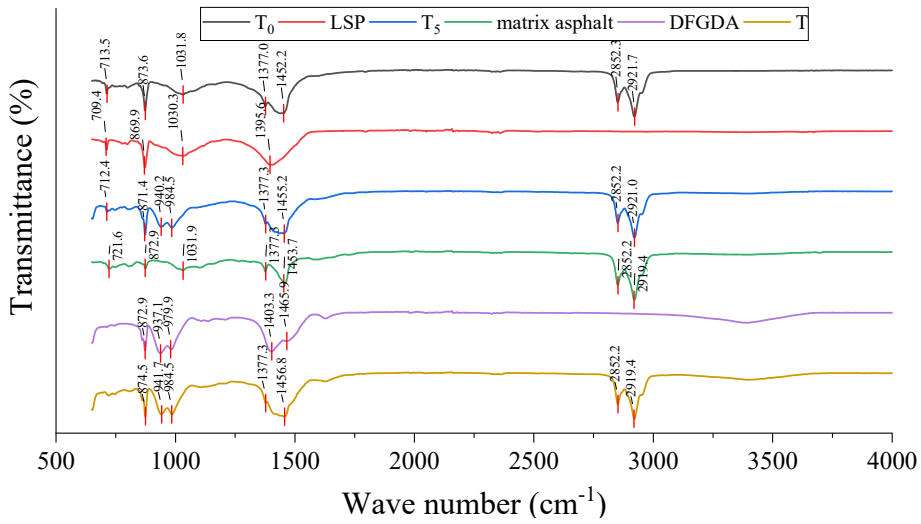

Figure 16. FTIR spectrum of filler (LSP, DFGDA), asphalt, and asphalt mortar (T_0, T_5, and T).

As shown in Figure 16, eight absorption peaks appeared in the DFGDA FTIR curve. Among them, 3400 cm^{-1} and 1625 cm^{-1} were the stretching vibrations and bending vibration bands of crystalline water, respectively; 1431 cm^{-1} and 876 cm^{-1} were the asymmetric stretching vibration and in-plane bending vibration bands of CO_3^{2-} in calcite, respectively;

1151 cm^{-1} and 654 cm^{-1} were the asymmetric stretching vibration and bending vibration bands of SO_4^{2-}, respectively; and 993 cm^{-1} and 947 cm^{-1} were the symmetric and asymmetric stretching vibration bands of SO_3^{2-}, respectively. A comparative observation of matrix asphalt, DFGDA, and T revealed no significant change in the spectrograms, no new peaks (i.e., no new functional groups), and no chemical reactions. The intensity of SO_3^{2-} absorption peaks at 993 cm^{-1} and 947 cm^{-1} in T did not change significantly, indicating that SO_3^{2-} in DFGDA was not thermally decomposed and maintained a stable state during the preparation of asphalt mastic. Similarly, the LSP also did not chemically react with the matrix asphalt, indicating similar action mechanisms for DFGDA asphalt mastic, DFGDA/LSP composite asphalt mastic, and LSP asphalt mastic. DFGDA and matrix asphalt were mainly physically mixed. Therefore, the performance of DFGDA asphalt mastic depended mainly on the degree of miscibility between DFGDA and matrix asphalt. By comparing the magnitudes of the characteristic peaks in the spectra of the three mastics, it could be seen that the DFGDA addition had a greater effect on the absorption peak at 1605 cm^{-1}, characterizing aromatic hydrocarbons and the benzene ring substitution region from 900 cm^{-1} to 650 cm^{-1} than LSP, which was the main reason for the changes in DFGDA-induced asphalt properties.

5. Conclusions

In this paper, the changes in high- and low-temperature rheological properties of DFGDA-added asphalt mastic were investigated at filler-to-asphalt mass ratios of 0.8, 1, and 1.2. The influence mechanism of DFGDA on the low-temperature properties of asphalt mastic was revealed through SEM and FTIR tests:

(1) The basic performance test of the DFGDA asphalt mastic showed enhanced consistency and hardness with the incorporation of DFGDA. The high-temperature performance of asphalt mastic was improved, while the low-temperature performance was reduced with increasing admixture.

(2) At the same temperature, with the increasing DFGDA admixture, the dynamic shear modulus of asphalt mastic was gradually improved, indicating that the elastic component of asphalt mastic became more extensive, and the deformation resistance was improved. The MSCR test at 70 °C indicated that with the increasing DFGDA admixture, the strain recovery ratio gradually rose, and irrecoverable creep flexibility decreased when other conditions were unchanged. The results implied that the increase of DFGDA admixture could improve the strain recovery rate and permanent deformation resistance of asphalt mastic. The BBR test demonstrated that the DFGDA incorporation adversely affected the low-temperature plastic deformation resistance of asphalt. However, the influence was inhibited by the growing DFGDA amount and the powder mastic ratio.

(3) Based on the Palierne model, an evaluation index C-value for the interaction capacity of asphalt and mineral powder was proposed. The interaction ability of DFGDA, LSP, and asphalt was evaluated using the C-value. It was concluded that DFGDA has a stronger ability to interact with asphalt than LSP.

(4) The FTIR test identified that the DFGDA incorporation did not produce new functional group vibrational bands. The DFGDA asphalt interface was dominated by physical interaction, and the performance of DFGDA asphalt mastic mainly depended on the miscibility between DFGDA and matrix asphalt. Due to its greater specific surface area, DFGDA improved the interaction ability of asphalt more significantly than LSP, thus obtaining better high-temperature performance. The SEM images showed voids between the DFGDA and asphalt, exerting a particularly negative impact on ductility and flexural creep modulus of strength.

In summary, DFGDA can be utilized as a novel filler in asphalt mastic, with guaranteed performance and effective alleviation of the disposal problem associated with DFGDA.

Author Contributions: K.L.: Methodology, Validation, Formal analysis, Resources, Writing—re-view & editing, Visualization, Supervision, Project. Z.Z.: Conceptualization, Methodology, Validation, Formal analysis, Investigation, Resources, Writing—review and editing, Visualization, Supervision, Project administration, Funding acquisition. Y.Z.: Investigation, Writing—review and editing, Visualization, Data curation. R.Y.: Conceptualization, Methodology, Supervision, Validation, Project administration. All authors have read and agreed to the published version of the manuscript.

Funding: This work has been supported by the National Natural Science Foundation of China (No. 51878079), Hunan Transportation Science and Technology Project (No. 201807), Postgraduate Scientific Research Innovation Project of Hunan Province (No. CX20190647). The authors gratefully acknowledge their financial support.

Institutional Review Board Statement: Not applicable.

Informed Consent Statement: Not applicable.

Data Availability Statement: All data, models, and code generated or used during the study appear in the submitted article.

Conflicts of Interest: The authors declare that they have no known competing financial interests or personal relationships that could have appeared to influence the work reported in this paper.

References

1. Al Mayyahi, A.; Sekar, A.; Rajendran, S.; Sigdel, S.; Lu, L.Y.; Wang, J.; Wang, G.H.; Li, J.; Amama, P.B. Hierarchical TiO_2-g-C_3N_4 photocatalyst with purification effect for NO_x oxidation under cyan light. *J. Photochem. Photobiol. A* **2023**, *444*, 114965. [CrossRef]
2. Al Mayyahi, A.; Sarker, S.; Everhart, B.M.; He, X.Q.; Amama, P.B. One-step fluorine-free synthesis of delaminated, OH-terminated Ti_3C_2: High photocatalytic NO_x storage selectivity enabled by coupling TiO_2 and Ti_3C_2-OH. *Mater. Today Commun.* **2022**, *32*, 103835. [CrossRef]
3. Cui, L.; Ba, K.; Li, F.; Wang, Q.; Ma, Q.; Yuan, X.; Mu, R.; Hong, J.; Zuo, J. Life cycle assessment of ultra-low treatment for steel industry sintering flue gas emissions. *Sci. Total Environ.* **2020**, *725*, 138292. [CrossRef] [PubMed]
4. Lisnic, R.; Jinga, S.I. Study on Current State And Future Trends Of Flue Gas Desulphurization Tehnologies: A Review. *Rev. Rom. Mater.* **2018**, *48*, 83–90. [CrossRef]
5. Liu, H.; Tan, Q.; Jiang, X.; Ma, S.; Liao, W.; Yang, F.; Huang, F. Comprehensive evaluation of flue gas desulfurization and denitrification technologies of six typical enterprises in Chengdu, China. *Environ. Sci. Pollut. Res. Int.* **2020**, *27*, 45824–45835. [CrossRef]
6. Burgess-Conforti, J.R.; Brye, K.R.; Miller, D.M.; Pollock, E.D.; Wood, L.S. Dry flue gas desulfurization by-product application effects on plant uptake and soil storage changes in a managed grassland. *Environ. Sci. Pollut. Res. Int.* **2018**, *25*, 3386–3396. [CrossRef] [PubMed]
7. Burgess-Conforti, J.R.; Miller, D.M.; Brye, K.R.; Pollock, E.D. Plant uptake of major and trace elements from soils amended with a high-calcium dry flue gas desulfurization by-product. *Fuel* **2017**, *208*, 514–521. [CrossRef]
8. Sheng, G.; Huang, P.; Mou, Y.; Zhou, C. Characteristics of fly ash from the dry flue gas desulfurization system for iron ore sintering plants. *Environ. Technol.* **2012**, *33*, 837–844. [CrossRef] [PubMed]
9. Lanzerstorfer, C.; Xu, Q.; Neuhold, R. Leaching of the residue from the dry off-gas de-dusting and desulfurization process of an iron ore sinter plant. *Int. J. Miner. Metall. Mater.* **2015**, *22*, 116–121. [CrossRef]
10. Li, J.; Qin, Y.R.; Zhang, X.Q.; Shan, B.L.; Liu, C.C. Emission Characteristics, Environmental Impacts, and Health Risks of Volatile Organic Compounds from Asphalt Materials: A State-of-the-Art Review. *Energ Fuel* **2024**, *38*, 4787–4802. [CrossRef]
11. Wu, R.; Dai, S.; Jian, S.; Huang, J.; Lv, Y.; Li, B.; Azizbek, N. Utilization of the circulating fluidized bed combustion ash in autoclaved aerated concrete: Effect of superplasticizer. *Constr. Build. Mater.* **2020**, *237*, 117644. [CrossRef]
12. Burgess-Conforti, J.R.; Brye, K.R.; Miller, D.M.; Pollock, E.D.; Wood, L.S. Land Application Effects of a High-Calcium, Dry Flue Gas Desulfurization By-Product on Trace Elements in Runoff from Natural Rainfall. *Water Air Soil Pollut.* **2018**, *229*, 34. [CrossRef]
13. Chen, L.; Tian, Y.; Stehouwer, R.; Kost, D.; Guo, X.; Bigham, J.M.; Beeghly, J.; Dick, W.A. Surface coal mine land reclamation using a dry flue gas desulfurization product: Long-term biological response. *Fuel* **2013**, *105*, 258–265. [CrossRef]
14. Chen, L.; Stehouwer, R.; Tong, X.; Kost, D.; Bigham, J.M.; Dick, W.A. Surface coal mine land reclamation using a dry flue gas desulfurization product: Short-term and long-term water responses. *Chemosphere* **2015**, *134*, 459–465. [CrossRef] [PubMed]
15. Zhang, Z.; Qian, J.; You, C.; Hu, C. Use of circulating fluidized bed combustion fly ash and slag in autoclaved brick. *Constr. Build. Mater.* **2012**, *35*, 109–116. [CrossRef]
16. Feng, X.H.; Wang, C.Q.; Ding, S.M. Performance of desulfurization ash for the preparation of grouting fire prevention material. *Environ. Sci. Pollut. Res. Int.* **2019**, *26*, 19228–19240. [CrossRef]
17. Li, X.-g.; Chen, Q.-b.; Huang, K.-z.; Ma, B.-g.; Wu, B. Cementitious properties and hydration mechanism of circulating fluidized bed combustion (CFBC) desulfurization ashes. *Constr. Build. Mater.* **2012**, *36*, 182–187. [CrossRef]
18. Sheng, G.; Li, Q.; Zhai, J. Investigation on the hydration of CFBC fly ash. *Fuel* **2012**, *98*, 61–66. [CrossRef]

19. Duan, S.; Liao, H.; Cheng, F.; Song, H.; Yang, H. Investigation into the synergistic effects in hydrated gelling systems containing fly ash, desulfurization gypsum and steel slag. *Constr. Build. Mater.* **2018**, *187*, 1113–1120. [CrossRef]
20. Woszuk, A.; Bandura, L.; Franus, W. Fly ash as low cost and environmentally friendly filler and its effect on the properties of mix asphalt. *J. Clean. Prod.* **2019**, *235*, 493–502. [CrossRef]
21. Cloutier, C.; Bautista, E.G.; Faheem, A.F.; Sobolev, K. Effect of Spray Dryer Absorbers as Mix Enhancer on HMA Performance. In Proceedings of the International Congress and Exhibition "Sustainable Civil Infrastructures: Innovative Infrastructure Geotechnology", Cairo, Egypt, 24–28 November 2018; pp. 80–95. [CrossRef]
22. Bautista, E.G.; Flickinger, J.; Saha, R.; Flores-Vivian, I.; Faheem, A.F.; Sobolev, K. Effect of Coal Combustion Products on high temperature performance of asphalt mastics. *Constr. Build. Mater.* **2015**, *94*, 572–578. [CrossRef]
23. Mistry, R.; Kumar Roy, T. Performance evaluation of bituminous mix and mastic containing rice husk ash and fly ash as filler. *Constr. Build. Mater.* **2021**, *268*, 121187. [CrossRef]
24. Chen, J.; Wu, S.; Pang, L.; Chen, Z.; Xie, J.; Lei, M. Influence of flue gas desulphurisation ash on moisture damage in asphalt mixtures. *Mater. Res. Innov.* **2014**, *18*, S4-81–S4-86. [CrossRef]
25. Wei, H.; Li, J.; Wang, F.Y.; Zheng, J.L.; Tao, Y.Y.; Zhang, Y.H. Numerical investigation on fracture evolution of asphalt mixture compared with acoustic emission. *Int. J. Pavement Eng.* **2022**, *23*, 3481–3491. [CrossRef]
26. Liu, Z.; Li, S.; Wang, Y. Characteristics of asphalt modified by waste engine oil/polyphosphoric acid: Conventional, high-temperature rheological, and mechanism properties. *J. Clean. Prod.* **2022**, *330*, 129844. [CrossRef]
27. Russo, F.; Veropalumbo, R.; Pontoni, L.; Oreto, C.; Biancardo, S.A.; Viscione, N.; Pirozzi, F.; Race, M. Sustainable asphalt mastics made up recycling waste as filler. *J. Environ. Manag.* **2022**, *301*, 113826. [CrossRef]
28. Zhang, H.; Gong, M.; Huang, Y.; Miljković, M. Study of the high and low-temperature behavior of asphalt based on a performance grading system in Northeast China. *Constr. Build. Mater.* **2020**, *254*, 119046. [CrossRef]
29. Xiang, L.; Cheng, J.; Que, G. Microstructure and performance of crumb rubber modified asphalt. *Constr. Build. Mater.* **2009**, *23*, 3586–3590. [CrossRef]
30. Ma, F.; Dai, J.; Fu, Z.; Li, C.; Wen, Y.; Jia, M.; Wang, Y.; Shi, K. Biochar for asphalt modification: A case of high-temperature properties improvement. *Sci. Total Environ.* **2022**, *804*, 150194. [CrossRef] [PubMed]
31. Palierne, J.F. Linear rheology of viscoelastic emulsions with interfacial tension. *Rheol. Acta* **1990**, *29*, 204–214. [CrossRef]
32. Graebling, D.; Muller, R. Determination of interfacial tension of polymer melts by dynamic shear measurements. *Colloids Surf.* **1991**, *55*, 89–103. [CrossRef]
33. Ziegel, K.D.; Romanov, A. Modulus Reinforcement in Elastomer Composites. I. Inorganic fillers. *J. Appl. Polym. Sci.* **1973**, *17*, 1119–1131. [CrossRef]
34. Rivera-Armenta, J.L.; Salazar-Cruz, B.A.; Chávez-Cinco, M.Y.; Morales-Cepeda, A.B.; Zapién-Castillo, S. Influence of chicken feather on the rheological properties and performance of modified asphalts. *Constr. Build. Mater.* **2020**, *264*, 120128. [CrossRef]